Structure and Electronic Properties of Cerium Orthophosphate: Theory and Experiment

Nicole Adelstein[1,3], B. Simon Mun[4], Hannah L. Ray[1,3], Phillip N. Ross Jr.[1], Jeffrey B. Neaton,[2] and Lutgard C. De Jonghe[1,3]

[1]Materials Sciences Division
[2]Molecular Foundry
Lawrence Berkeley National Laboratory, 1 Cyclotron Road, Berkeley CA 94720, USA

[3]Department of Materials Science and Engineering
University of California at Berkeley, Berkeley CA 94720, USA

[4]Department of Applied Physics
Hanyang University, ERICA, Gyeonggi 426-791 Republic of Korea

Abstract

Structural and electronic properties of cerium orthophosphate ($CePO_4$) are calculated using density functional theory (DFT) with the local spin-density approximation (LSDA+*U*), with and without gradient corrections (GGA-(PBE)+*U*), and compared to X-ray diffraction and photoemission spectroscopy measurements. The density of states is found to change significantly as the Hubbard parameter *U*, which is applied to the Ce 4f states, is varied from 0 to 5 eV. The calculated structural properties are in good agreement with experiment and do not change significantly with *U*. Choosing *U* = 3 eV for LDSA provides the best agreement between the calculated density of states and the experimental photoemission spectra.

I. Introduction

New materials with high proton conductivities in the temperature range 300-500°C can be of benefit as solid electrolytes in a variety of electrochemical devices such as hydrogen sensors, hydrogen separation membranes, and fuel cells. Incorporation of such a material into a fuel cell would, for example, facilitate the *in-situ* reforming of liquid biofuels and reduce the need for noble catalysts. Rare-earth phosphates have been investigated for this purpose because of their stability at high

temperatures, and their ability to incorporate protons when doped with aliovalent cations [1-4].

Recent AC impedance spectroscopy for $CePO_4$ [2] indicates a total conductivity an order of magnitude higher than that of $LaPO_4$, the known proton-conductor. The enhanced conductivity of $CePO_4$ relative to its La-based counterpart has been attributed to hole conduction, based on defect chemistry interpretations of the measured conductivity in both wet versus dry conditions and reducing versus oxidizing environments [2]. First-principles calculations using density functional theory (DFT) can potentially reveal the differences between $CePO_4$ and $LaPO_4$ conductivities. However, whereas ground-state electronic structure and proton conduction have already been studied with DFT for $LaPO_4$ [5], the electronic structure of $CePO_4$ is relatively unexplored. In this work, we determine the ground state electronic structure of $CePO_4$ using DFT and compare it to X-ray diffraction measurements and photoemission spectroscopy.

Cerium can exist in both the 3^+ and 4^+ oxidation states. The nominal charge on cerium in $CePO_4$ is Ce^{3+}, leaving one highly localized 4f electron on each cerium atom. The highly correlated and localized nature of these 4f states demands special consideration for the electronic structure of $CePO_4$. For cerium oxides, many groups [6-9] have recently documented the failure of standard DFT within the local density or generalized gradient approximations (LDA and GGAs) due to significant self-interaction errors associated with 4f electron states. For example, these groups report erroneous structural parameters or even metallic behavior for Ce-based compounds that are known to be insulators [10]. A common approach to address these deficiencies is the DFT + *U* method [11]. In the DFT + *U* framework, the strong Coulomb repulsion between localized *4f* states in Ce is treated by adding a Hubbard term to the effective potential, leading to an improved description of correlation effects in transition-metal oxides. DFT + *U* requires two parameters, the Hubbard parameter *U* and the exchange interaction *J*. Since there is no unique way of including a Hubbard term within the DFT framework[11], different approaches may be

adopted. In what follows, we use the rotationally invariant method of Dudarev *et al*. [12], which is described in Section III, Computational Methods.

Appropriate values of *U* for Ce 4f electrons have been debated in the literature, and reported values for cerium oxides range from *U*=3-6 eV for LDA and *U*=1.5-5 eV for GGA [6, 7, 13, 14]. Fabris *et al*. [7], for example, used a linear response approach [15] for CeO_2 and Ce_2O_3 and found *U* = 3 eV (LDA) and 1.5 eV (GGA). All studies noted that both the electronic structure and lattice parameters were somewhat sensitive to the value of *U*, although in different ways for CeO_2 and Ce_2O_3, indicating that the best choice for *U* may depend on the environment of the cerium atom.

In this study, ground-state structure and electronic properties of $CePO_4$ are computed using DFT+*U* for several different values of *U* and compared with X-ray diffraction (XRD), X-ray photoemission spectrometry (XPS), and AC impedance spectroscopy experiments on sintered, polycrystalline samples. We propose an optimal value of *U* that agrees with measured photoemission near the valence band edge, and show that this value of *U* provides structural parameters that agree well with those obtained by XRD, thus providing a necessary foundation for future calculations into electronic and protonic conductivity in $CePO_4$.

II. Experimental Methods

Cerium orthophosphate powders, purchased from Alfa Aesar, are heat treated for 1 hour at 800°C in order to convert from the hydrated rhabdophane to the monoclinic phase. Powders are ground and sieved through 325 mesh, and then ball milled in isopropyl alcohol with 2 wt% PolyvynalVB, DiButal Phthalate, Manhaden Fish Oil (from Aldrich, Mallinckrodt, and Sigma, respectively) for a 24 hours. The powders are dried, ground, and sieved again, and then uniaxially die pressed at 2000 psi into pellets. Pellets are heated to 600°C for 1h to remove binders and then heated to 1200°C for 5 hours for sintering. X-ray diffraction scans of powders and pellets are performed on a Philips PW3040 X'Pert Pro diffractometer using the Cu Kα (λ = 1.5406 Å) source operated with a 45 keV X-ray tube voltage.

A Kratos AXIS-NOVA Hemispherical electron analyzer is used for the measurement of XPS. The monochromatic Al K_α (photon energy =1486.6eV) is used as the x-ray source, and the total energy resolution is set to ~0.4 eV. The pass energy and dwell time of photoemission spectra is set to 20 eV and 100 msec, respectively. Prior to the XPS measurement, the sample surface is lightly sputtered with argon to remove any surface contamination. Sputtering does not change the oxidation state, as was shown by Glorieux in the $CePO_4$ spectra of the 3d binding energies [16]. A small charging effect is present during the measurement, and a low-energy electron flood gun is utilized when necessary. All elements in the sample are identified from a survey scan and the chemical state of each element is also confirmed. In order to compare the DFT density of states to the photoemission spectra, the Shirley background is subtracted from measured valence band spectra to remove the effects of inelastic scattering [17].

III. Computational methods

To compute the structure and electronic properties of $CePO_4$, we use DFT+*U* with both the local spin-density approximation (notated here as LDA) and the spin-dependent generalized gradient approximation (GGA) [18]. All results are obtained using the projector augmented-wave (PAW) method [19] as implemented in the Vienna *ab initio* Simulation Package (VASP) [20-22]. For comparison with XPS, a PBE0 hybrid functional is also employed [23]. We treat explicitly 12 electrons for cerium ($5s^25p^66s^25d^14f^1$), 5 for phosphorus ($2s^22p^5$), and 6 for oxygen ($2s^22p^6$). Brillouin zone integrations are performed with a Gaussian broadening of 0.1 eV during all calculations, a 6x6x6 Monkhorst-Pack k-point mesh with the original packing scheme [24], and a 600 eV plane-wave cutoff, all of which result in good convergence of the ground-state properties reported here. Energies are converged to 10^{-6} eV and Hellmann-Feynman forces on the ions are converged to 10 meV/Å. The equilibrium cell volume and shape are determined by optimizing all internal degrees of freedom with different functionals and values of *U*. The bulk modulus is calculated two ways, first by relaxing the ion position only and second by relaxing the shape and ion positions. Both values are found to be consistent, and the latter is reported. The

range of volumes used for the bulk modulus calculations is within 4-5% of the minimum volume.

As described above, it is well known that the LDA, with or without gradient corrections, may incorrectly capture the electronic structure of materials with localized d or f states. In this work, we use DFT+U to correct for self-interaction errors associated with the Ce 4f states. This approach is described by Dudarev *et al.* [12] where only an effective Hubbard parameter $U_{\text{eff}} = U - J$ enters the Hamiltonian. Here, we vary U_{eff} (which we simply refer to as U from here on) from 0 to 5 eV. (The standard DFT result corresponds to U=0 eV.)

$CePO_4$ is known to be an antiferromagnet below 77K [25]. The lowest energy magnetic ordering is determined within our spin-polarized DFT+U calculations. Since there are four cerium atoms in the unit cell, for antiferromagnetic ordering two must be spin-up and two must be spin-down (Fig 1, Section III).

IV. Results and Discussion

A. Structural

The monoclinic phase of $CePO_4$ assumes a structure with $P2_1/n$ symmetry (Fig 1) [26].

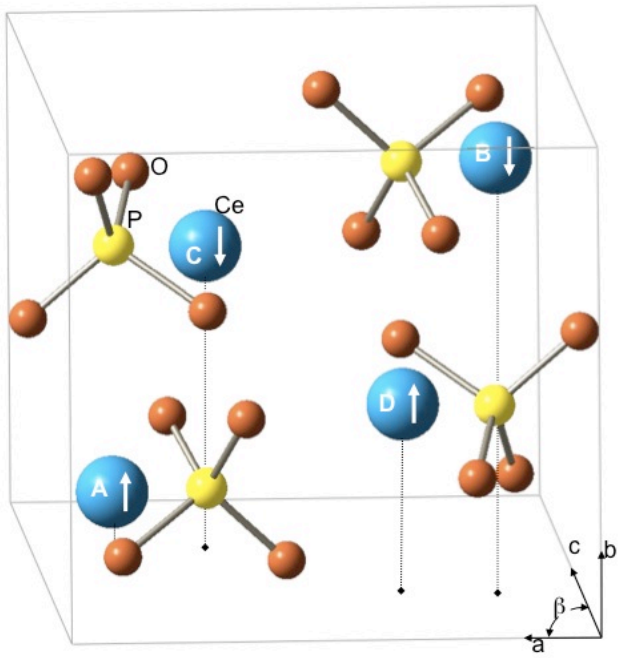

Figure 1: The conventional $CePO_4$ unit cell. The lattice vectors are **a**, **b**, and **c**, while the angle between **a** and **c** is β. The cerium cations are shown in blue, the tetrahedra are made of orange oxygen atoms and yellow phosphorus atoms. An antiferromagnetic spin ordering of the cerium atoms is indicated with up and down arrows.

All atoms sites have the same symmetry in the 4e Wyckoff position, with coordinates: 'A' (x,y,z), 'B' (-x,-y,-z), 'C' (-x+1/2,y+1/2,-z+1/2), and 'D' (x+1/2,-y+1/2,z+1/2). There is a single unique cerium site, one phosphorous site, and four oxygen sites. For U=0, the lowest energy is ferromagnetic and for any finite U the lowest energy is antiferromagnetic. A small but non-negligible amount of hybridization between cerium 4f and oxygen 2p suggests that the antiferromagnetic ordering found for finite values of U is mediated by superexchange. In the antiferromagnetic ground state, each cerium atom has six cerium nearest neighbors; two neighbors are spin-aligned and four are anti-aligned.

As expected, we find that LDA+U functionals result in smaller lattice parameters than the experiment for all values of U tested, leading to a 7% smaller volume than the experiment. In contrast, GGA-PBE predicts larger lattice parameters for all values of U, leading to overestimation of the experimental volume by at most 4%, as

shown in Fig 2 and Table 1a, which also show the LDA+*U* data. In all cases, computed Wyckoff positions are in very good agreement with experiment, as can be seen for selected *U* in Table 1b.

Table 1a: The volume and lattice parameters for the measured and calculated $CePO_4$ unit cell for all *U*. The experiemtnal bulk modulus (BM) for is not known (NA).

Functional	Volume (Å^3)	a (Å)	b (Å)	c (Å)	β (deg)	BM (GPa)
Experiment	300.60	6.8004	7.0231	6.4717	103.460	NA
LDA U=0	287.37	6.6935	6.9266	6.3705	103.357	125
U=1	287.98	6.6999	6.9302	6.3740	103.331	132
U=2	289.46	6.7083	6.9465	6.3897	103.561	129
U=3	290.20	6.7141	6.9515	6.3934	103.464	129
U=4	290.99	6.7181	6.9597	6.3993	103.455	133
U=5	291.51	6.7204	6.9616	6.4040	103.351	133
PBE U=0	308.42	6.8956	7.0893	6.4980	103.849	99
U=1	309.20	6.8944	7.0981	6.5079	103.862	100
U=2	309.80	6.9263	7.0741	6.5166	104.010	99
U=3	310.84	6.9091	7.1084	6.5195	103.883	103
U=4	311.65	6.9138	7.1174	6.5245	103.908	102
U=5	312.38	6.9156	7.1235	6.5304	103.832	103

1b: Atom positions for selected values of *U.*

		Experiment	LDA U=0	LDA U=3	PBE U=0	PBE U=3
Ce	x	0.2818	0.2800	0.2813	0.2852	0.2860
	y	0.1591	0.1587	0.1586	0.1583	0.1586
	z	0.1000	0.1032	0.1023	0.0992	0.0991
P	x	0.3050	0.3039	0.3047	0.3039	0.3046
	y	0.1663	0.1642	0.1641	0.1621	0.1621
	z	0.6124	0.6144	0.6136	0.6116	0.6111
O1	x	0.2494	0.2486	0.2494	0.2498	0.2505
	y	0.0059	0.0041	0.0047	0.0057	0.0061
	z	0.4439	0.4438	0.4433	0.4405	0.4405
O2	x	0.3813	0.3817	0.3827	0.3813	0.3822
	y	0.3314	0.3343	0.3333	0.3311	0.3303
	z	0.4995	0.4964	0.4959	0.4987	0.4984
O3	x	0.1061	0.4771	0.4770	0.4714	0.4714
	y	0.2163	0.1067	0.1084	0.1034	0.1035
	z	0.8040	0.8096	0.8089	0.8067	0.8061
O4	x	0.1282	0.1243	0.1256	0.1273	0.1282
	y	0.2163	0.2158	0.2158	0.2124	0.2125
	z	0.7086	0.7152	0.7136	0.7099	0.7086

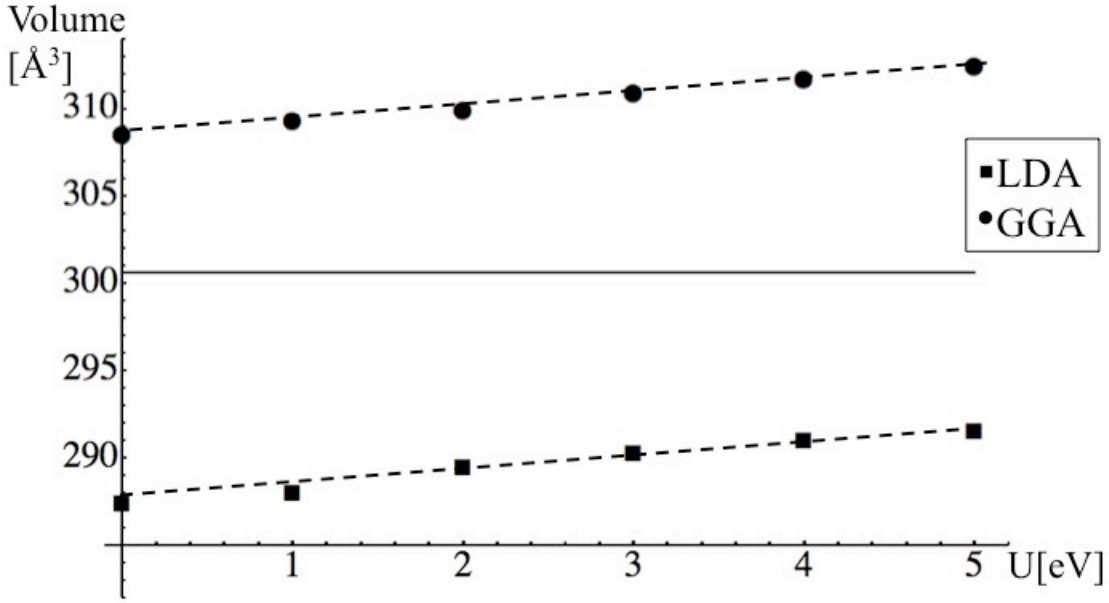

Fig 2: Over the range of *U* = 0-5 eV, neither LDA nor GGA predicts the experimental volume, as indicated by the black line.

A primary conclusion of our study of the trends in computed lattice parameters with respect to *U* is that a larger value of *U* results in a larger unit cell volume. This result will be discussed later. It might be proposed to obtain the experimental volume if a high enough value of *U* for LDA calculations were chosen, but such a high choice of *U* would give an unreasonable electronic structure when compared to the XPS data, as will be shown in the next section.

The geometry and structural parameters do not depend significantly on the choice of *U*. The angle β is calculated to be between 103.3 and 103.6 degrees for LDA, which brackets the experimental value of 103.47 degrees. For GGA-PBE, the range of β values is between 103.8 and 104.0 degrees. The angle β is labeled in the figure of the unit cell, Fig 1, and the calculated values are given in Table 1a. Since the LDA seems to predict the angle β better and neither functional gives a perfectly accurate value for the volume, the LDA functional will be used for future calculations. The experimental bulk modulus is not known, but the calculated values for GGA-PBE

range between 99 and 103 GPa and the LDA values range between 123 and 133 GPa (Table 1a).

There is little variation in the structural parameters with change in *U* besides the general increase in volume with *U* and slight increase in bulk modulus. Comparison of calculated structural parameters to experiment does not point to a single 'best' value of *U*, so in what follows, we suggest an optimal *U* for Ce in $CePO_4$ through comparison to measured photoemission spectra.

B. Electronic Structure

In contrast to the lattice parameters, the computed electronic structure depends significantly on the value of *U*, such that at *U*=0 eV, $CePO_4$ is metallic and ferromagnetic but at finite values of *U* it is insulating and antiferromagnetic. For all values of *U* the band gap and the gap between the first two valence bands is calculated using energy levels at the high symmetry k-point M=(-0.5,0,0.5), which represents the location of the direct band gap, as shown in Fig 3. The band gap increases with increasing *U*, which can also be seen in the density of states for selected U (Fig 4). There is sharp peak at the Fermi energy due to the Ce 4f electron in the 3+ state, which was assigned using the partial density of states. Note also that the gap between this Ce 4f orbital and the top of the oxygen 2p band decreases with increasing *U* (peaks labeled in Fig 3 at top of Fig 4). The energy difference between these two peaks will be compared to XPS.

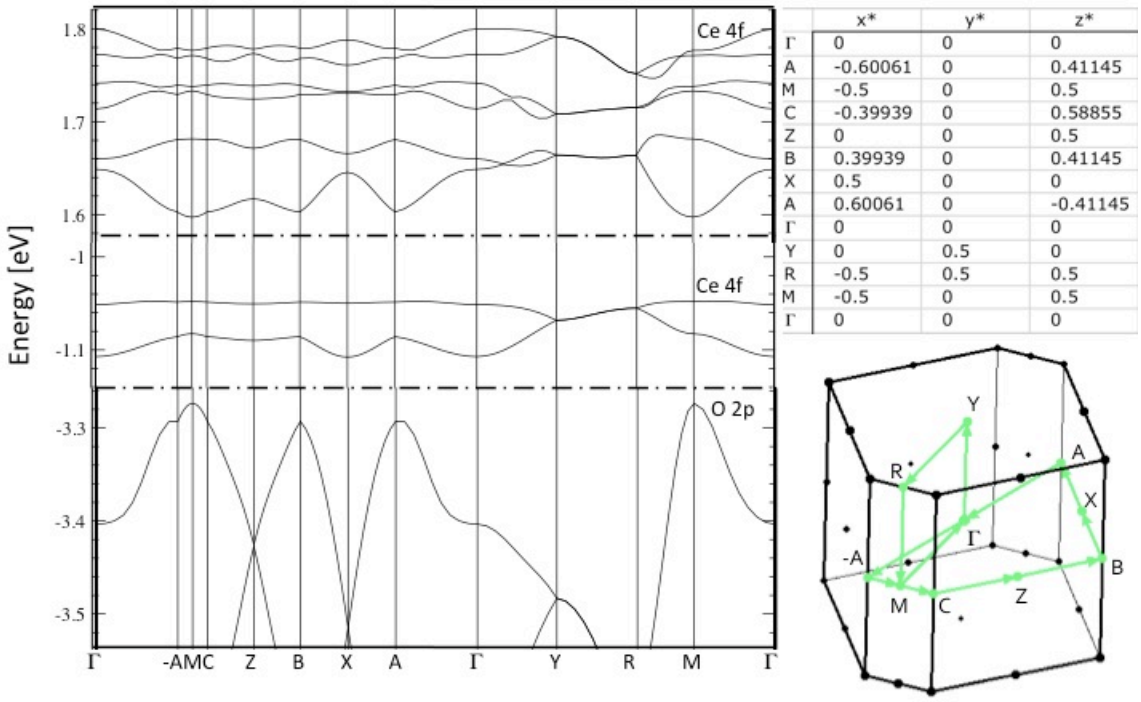

	x*	y*	z*
Γ	0	0	0
A	-0.60061	0	0.41145
M	-0.5	0	0.5
C	-0.39939	0	0.58855
Z	0	0	0.5
B	0.39939	0	0.41145
X	0.5	0	0
A	0.60061	0	-0.41145
Γ	0	0	0
Y	0	0.5	0
R	-0.5	0.5	0.5
M	-0.5	0	0.5
Γ	0	0	0

Figure 3: The band structure for LDA U=3 eV was calculated along lines between high symmetry points in the first Brillouin Zone, which are given in the table and plot to the left. High symmetry points are provided in reduced coordinates of the primative reciprocal lattice vectors.

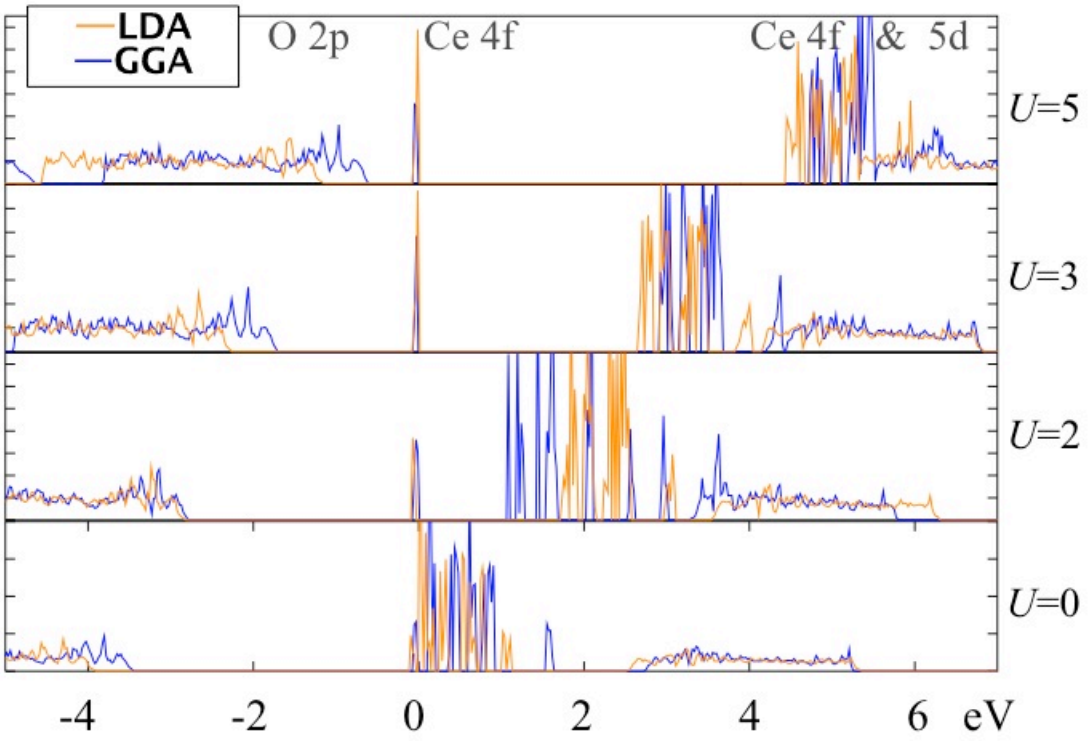

Figure 4: The valence and conduction bands for *U*=0, 2, 3 and 5 eV; the other values of *U* follow this trend. The orange is the LDA functional and the blue is the GGA functional. The Fermi Energy is set to 0 eV and the orbital assignments at the top of the plot are from the partial DOS (which is not shown).

The energy gap between the Ce 4f and the top of the oxygen 2p valence bands is measured with XPS to be 2.5 +/- 0.2 eV, which corresponds to a value of *U* = ~3 eV for LDA and *U*= ~2.5 eV for GGA, as shown in Fig 5. The agreement between the XPS of the valence bands and the LDA+*U*=3eV density of states is remarkably good, as will be shown later (Fig 9).

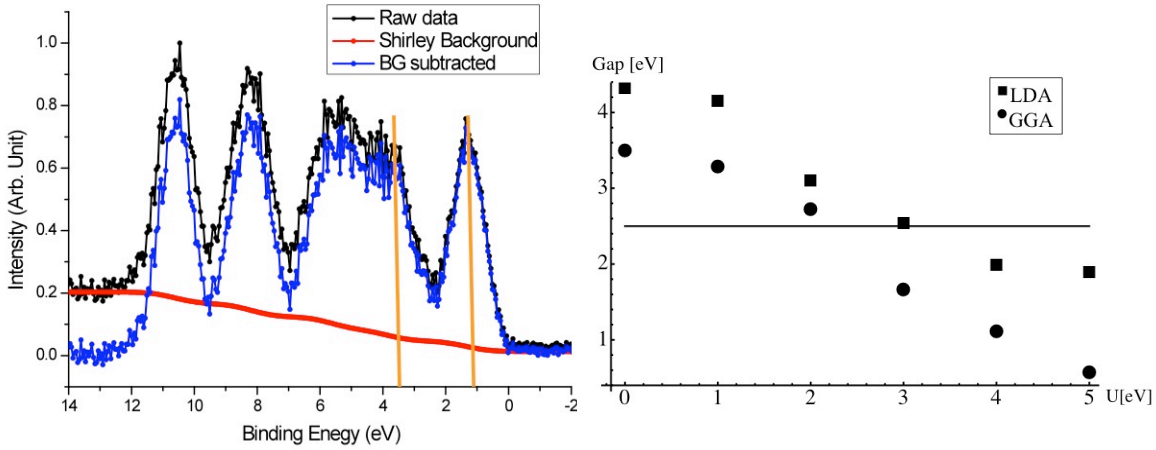

Figure 5a: The energy difference between the first two valence bands, measured peak to peak, is 2.5 +/- 0.2 eV. 5b: The energy difference between these two bands as measured by DFT+*U* for *U*=0-5 eV is plotted for LDA and GGA.

The valence gap does not decrease linearly with increasing *U* and contains an inflection point for both LDA and GGA. The effective Hubbard *U* is only added to the cerium f orbitals and serves to increase their localization and decrease their overlap with oxygen orbitals, which most likely causes the decrease in the gap between the cerium and oxygen valence bands. The plot of valence gap versus *U* for LDA shows a leveling off of the gap after *U* = 4 eV, which implies that this value of *U* is large enough to completely localize the 4f orbitals and larger values will not significantly change the electronic structure. This "leveling off" is not yet seen for GGA, though this may not be surprising since the inflection point in Fig 5 for GGA occurs at a high value for *U* than for LDA.

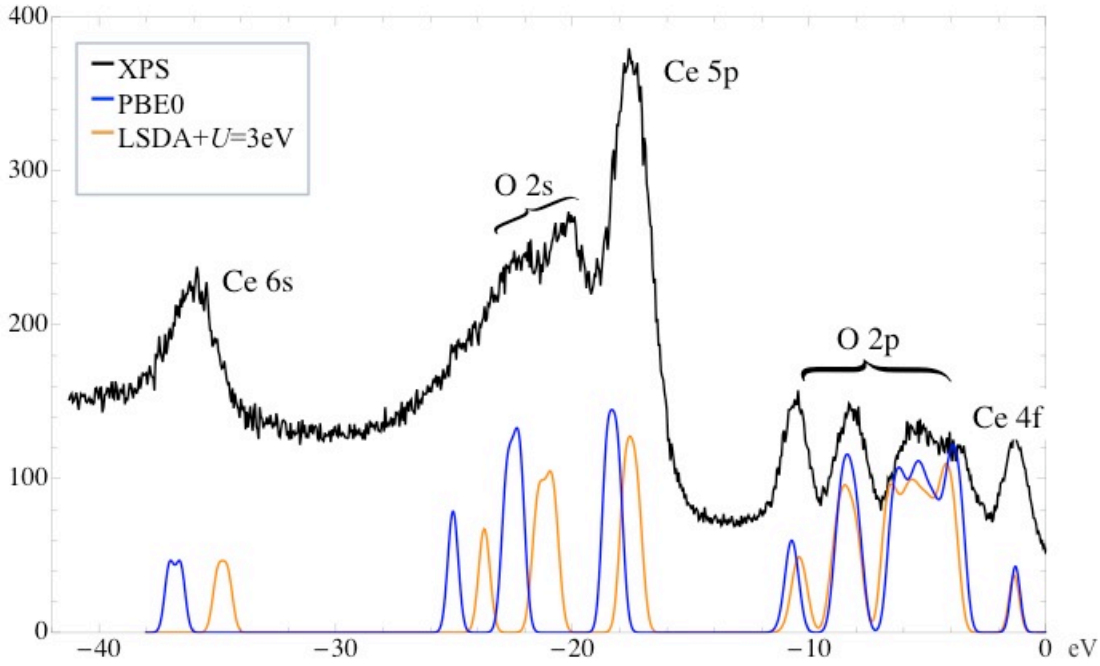

Figure 6: The valence band photoemission spectra is plotted along with the calculated partial density of states with Gaussian smearing for the LDA+*U*=3eV and PBE0 functionals. The peaks are labeled from the calculated partial density of states and are supported by known XPS binding energies.

The photoemission spectrum near the Fermi energy is best fitted to a DFT valence band using *U*=3 eV for LDA, as shown in Figs 5 and 6. The XPS peaks in Fig 6 are assigned using the partial DOS (not shown), and match the known literature values of the binding energies (calibrated using the Ce *3d* peaks) [27]. The excellent agreement found using the LDA+*U*=3eV functional is checked with the PBE0 functional, which contains 25% Hartree-Fock exact exchange [23]. Exact agreement between the XPS spectrum and the LDA+*U* density of states is not expected because the on-site interaction was only added to the cerium f orbitals. Including some degree of exact exchange stretches out the DOS, and yields better agreement between the low energy cerium 6s orbital and XPS, but worse agreement between the oxygen 2s orbitals and XPS. There is little difference between the valence bands for LDA+*U*=3eV versus PBE0, indicating that *U*=3eV is adaquate to describe these orbitals. In addition, spin-orbit coupling calculations are performed for LDA+*U*=0

and LDA+U=3, and a 3 eV splitting of the Ce 5p orbitals is observed, which is not seen in photoemission measurments due to its proximity to the O 2s orbitals. Further, we find that there spin-orbit coupling has little to no influence on the electronic structure near the valence band edge.

Two additional calculations are performed to better understand the correlation between the cell volume, the functional, and the magnitude of U. The density of states calculated using LDA+U=3eV is computed for both the LDA+U=3eV equilibrium unit cell volume (290.20 Å^3) and for the GGA+U=3eV minimum energy volume (290.20 Å^3). These density of states are then compared to the density of states calculated using GGA+U=3eV at both volumes (290.20 Å^3 and 290.20 Å^3). The valence band does not change significantly for the LDA and GGA density of states with different volumes, but with the larger volume, the gap between the valence cerium 4f and oxygen 2p decreases by about 0.5 eV due to less overlap between orbitals, as is evident in Fig 7.

A comparison of LDA and PBE at U=3eV for the same volume shows some change in the valence and conduction bands. There is a slight change in the gap (0.25 eV) and an even smaller change in the valence band gap (0.17 eV). These additional experiments indicate the smaller valance gap in GGA versus LDA is due to mainly the volume, but the type of functional also plays a small role.

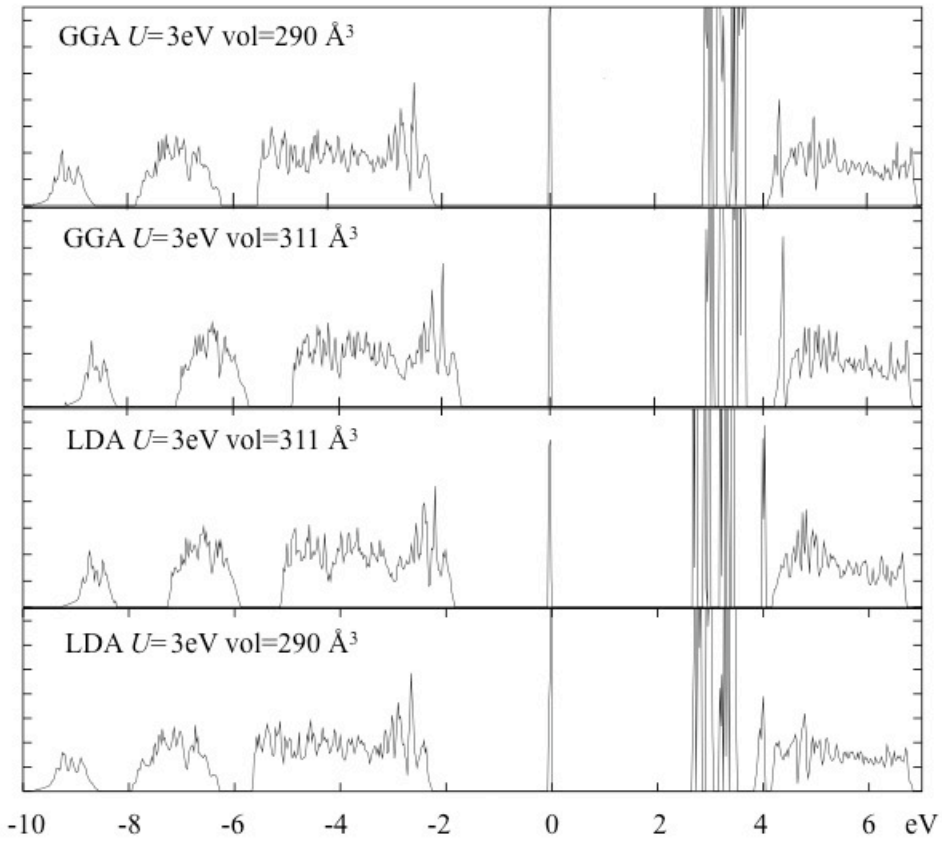

Figure 7: The density of states near the top of the valence band (set to zero in each case) is plotted for GGA and LDA+*U*=3 eV for a unit cell with volume = 290 Å^3 and with volume = 311 Å^3.

IV. Conclusions

The ground state electronic structure of $CePO_4$ was investigated with XPS and DFT plus an empirical *U* parameter for LDA and GGA functionals. By direct comparison with experiments, we found that the Hubbard *U* parameters for Ce 4f states in $CePO_4$ that provide the best match for experiments were *U*=3 for LDA functional and *U*=2 for the GGA-PBE functional. All the peaks in the XPS could be identified with the DFT partial density of states and correspond to known binding energies. The use of the non-empircal PBE0 functional to calculate the density of states confirmed that adding *U*=3eV to the LDA accurately offsets self-interaction energy errors in common exchange-correlation functionals. Spin-orbit coupling did not affect

electronic structure near the valence band edge, and thus was not necessary in chosing an appropriate value of *U*.

The DOS depended significantly on the value of *U* whereas the materials properties (volume, symmetry, and bulk modulus) did not depend significantly *U*, though the choice of functional affected the volume and thus the electronic structure. We found that the smaller value of *U* necessary for the GGA versus LDA functional is due to the functional as well as the unit cell volume.

The calculations presented here show the importance of the choice of an emperically based *U*. In particular, we found that the difference in the appropriate value of *U* between LDA and GGA was less than 1 eV, whereas work on other cerium oxides showed greater difference, such as 1.5 eV with the linear response method [7].

These DFT calculations set the stage for further theoretical work on proton hopping in $CePO_4$ and the electronic structure of aliovalently doped and oxygen deficient $CePO_4$, and will inevitable lend insight into the nature of the mixed-conduction of this proton-conducting material.

Acknowledgments

This work was supported by the Director, Office of Science, Office of Basic Energy Sciences, Materials Sciences and Engineering Division, of the U.S. Department of Energy under Contract No. DE-AC02-05CH11231. Work at the Molecular Foundry was supported by the Office of Science, Office of Basic Energy Sciences, of the U.S. Department of Energy under Contract No. DE-AC02-05CH11231. We also gratefully acknowledge computational support from NERSC, which is supported by the Office of Science of the U.S. Department of Energy under Contract No. DE-AC03-76SF00098.

1. T. Norby, Nature **410** (6831), 877-878 (2001).
2. N. Kitamura, K. Amezawa, Y. Tomii, T. Hanada, N. Yamamoto, T. Omata and S. Otsuka-Yao-Matsuo, J. Electrochem. Soc. **152** (4), A658-A663 (2005).
3. E. G. del Moral, D. P. Fagg, E. Chinarro, J. C. C. Abrantes, J. R. Jurado and G. C. Mather, Ceram. Int. **35** (4), 1481-1486 (2009).

4. G. Harley, K. D. Kreuer, J. Maier and L. C. De Jonghe, J. Non-Cryst. Solids **355** (16-17), 932-937 (2009).
5. R. Yu and L. C. De Jonghe, J Phys Chem C **111** (29), 11003-11007 (2007).
6. J. L. F. Da Silva, M. V. Ganduglia-Pirovano, J. Sauer, V. Bayer and G. Kresse, Phys Rev B **75** (4) (2007).
7. S. Fabris, S. de Gironcoli, S. Baroni, G. Vicario and G. Balducci, Phys. Rev. B **71** (4) (2005).
8. J. Kullgren, C. W. M. Castleton, C. Muller, D. M. Ramo and K. Hermansson, J. Chem. Phys. **132** (5) (2010).
9. G. Pacchioni, J. Chem. Phys. **128** (18) (2008).
10. K. Terakura, T. Oguchi, A. R. Williams and J. Kubler, Phys Rev B **30** (8), 4734-4747 (1984).
11. V. I. Anisimov, F. Aryasetiawan and A. I. Lichtenstein, J. Phys.-Condes. Matter **9** (4), 767-808 (1997).
12. S. L. Dudarev, G. A. Botton, S. Y. Savrasov, Z. Szotek, W. M. Temmerman and A. P. Sutton, Phys. Status Solidi A-Appl. Res. **166** (1), 429-443 (1998).
13. J. L. F. Da Silva, M. V. Ganduglia-Pirovano and J. Sauer, Phys Rev B **76** (12) (2007).
14. C. Loschen, J. Carrasco, K. M. Neyman and F. Illas, Phys Rev B **75** (3) (2007).
15. M. Cococcioni and S. de Gironcoli, Phys Rev B **71** (3) (2005).
16. B. Glorieux, R. Berjoan, M. Matecki, A. Kammouni and D. Perarnau, Appl. Surf. Sci. **253** (6), 3349-3359 (2007).
17. M. Repoux, Surf. Interface Anal. **18** (7), 567-570 (1992).
18. J. P. Perdew, K. Burke and M. Ernzerhof, Phys. Rev. Lett. **77** (18), 3865-3868 (1996).
19. P. E. Blochl, Phys Rev B **50** (24), 17953-17979 (1994).
20. G. Kresse and J. Furthmuller, Comput. Mater. Sci. **6** (1), 15-50 (1996).
21. G. Kresse and J. Furthmuller, Phys. Rev. B **54** (16), 11169-11186 (1996).
22. G. Kresse and J. Hafner, Phys Rev B **47**, 558 (1993).
23. C. Adamo and V. Barone, J. Chem. Phys. **110** (13), 6158-6170 (1999).
24. H. J. Monkhorst and J. D. Pack, Phys. Rev. B **13** (12), 5188-5192 (1976).
25. F. D. Srygley and W. L. K., Bulletin of the American Chemical Society **24** (2) (1979).
26. G. W. Beall, L. A. Boatner, D. F. Mullica and W. O. Milligan, Journal of Inorganic & Nuclear Chemistry **43** (1), 101-105 (1981).
27. A. Fujimori, Phys Rev B **28** (8), 4489-4499 (1983).